International Journal of Thermofluids 22 (2024) 100700

Contents lists available at ScienceDirect

International Journal of Thermofluids

journal homepage: www.sciencedirect.com/journal/international-journal-of-thermofluids

Enhancing the efficacy of humidifier-dehumidifier desalination in humid regions through the use of an absorption refrigeration cycle (an economic and experimental investigation)

Sherzod Abdullaev [a,b,*], Barno Sayfutdinovna Abdullaeva [c], Serikzhan Opakhai [d], Laith H. Alzubaidi [e,f,g]

[a] Faculty of Chemical Engineering, New Uzbekistan University, Tashkent, Uzbekistan
[b] Department of Science and Innovation, Tashkent State Pedagogical University named after Nizami, Tashkent, Uzbekistan
[c] Department of Mathematics and Information Technologies, Faculty of Mathematics and Physics, Vice-Rector for Scientific Affairs, Tashkent State Pedagogical University, Tashkent, Uzbekistan
[d] Faculty of Physics and Technical science, L.N. Gumilyov Eurasian National University, Astana, 010000, Kazakhstan
[e] College of technical engineering, the Islamic University, Najaf, Iraq
[f] College of technical engineering, the Islamic University of Al Diwaniyah, Al Diwaniyah, Iraq
[g] College of technical engineering, the Islamic University of Babylon, Babylon, Iraq

ARTICLE INFO

Keywords:
Desalination system
Humidifier-dehumidifier
Hybrid heater
Vapor absorption refrigerator
Photovoltaic panel
Humid regions

ABSTRACT

This experimental study investigates the performance of a novel humidifier-dehumidifier (HDH) desalination system integrated with a vapor absorption refrigerator (VAR) and photovoltaic (PV) panels for humid regions. The effects of air mass flow rate ($\dot{m}_a$) and inlet air temperature on key performance indicators were evaluated. Increasing $\dot{m}_a$ from 0.0039 kg/s to 0.0071 kg/s led to a 73 % increase in freshwater output, a 35 % increase in Coefficient of Performance (COP), a 100 % increase in Gain of Output Ratio (GOR), and a 75 % increase in Recovery Ratio (RR), but a 20 % decrease in dehumidifier efficiency. The maximum freshwater production rate of 870 g/h and a GOR of 1.4 were obtained at $\dot{m}_a$= 0.0071 kg/s and inlet air temperature of 50 °C, representing a 117 % increase compared to the lowest temperature and flow rate tested. The cost of freshwater for solar and electric operation modes was 0.075 and 0.094 USD/kg, respectively. The system's novelty lies in the integration of HDH desalination with a VAR and PV system, enabling continuous freshwater production even under cloudy or nighttime conditions. The findings demonstrate the potential of the proposed system for sustainable freshwater production in humid areas.

1. Introduction

Fresh water has been the most vital resource for human life throughout history [1]. Access to clean, potable water is essential for sustaining human populations, agriculture, and industry. The main challenge facing human settlements is ensuring a reliable supply of fresh water to meet their needs. Different regions of the globe have varying climates, which directly affects the availability and quality of water resources in those areas [2]. Some regions are blessed with abundant freshwater sources, while others have limited or non-freshwater supplies, such as saline groundwater, brackish lakes, or polluted surface water [3]. In the past, the location of many civilizations was heavily influenced by the proximity to reliable freshwater sources. The siting of cities and villages was often a result of strategic decisions made by past populations to ensure access to this precious resource. However, the rapid growth of industry and human populations in recent decades has placed immense strain on freshwater resources in many parts of the world [2]. In areas where local water supplies cannot meet the escalating demand, alternative sources of freshwater must be tapped, often through energy-intensive desalination processes [3]. Seawater, brackish groundwater, and polluted surface waters can all be treated and converted into potable freshwater using various technologies [4]. The selection of the most appropriate desalination technology for a given region depends on a variety of factors, including geographic location, climate, population size, and industrial activity [5]. Considerations such as available energy sources, environmental impacts, and economic feasibility must also be carefully weighed when choosing the optimal

* Corresponding author.
E-mail address: sherzodbek.abdullaev.1001@gmail.com (S. Abdullaev).

https://doi.org/10.1016/j.ijft.2024.100700

Available online 22 May 2024

Nomenclature

Abbreviation

COP	Coefficient of Performance
DCS	Desiccant Cooling System
GOR	Gain of Output Ratio
HDH	Humidifier-Dehumidifier
MED	Multi-Effect Distillation
MSF	Multi-Stage Flash
ORC	Organic Rankine Cycle
OWCA	Open Water-Closed Air
OWOA	Open Water-Open Air
PV	Photovoltaic
RO	Reverse Osmosis
RR	Recovery Ratio
SSD	Single-Slope Distillation
VAR	Vapor Absorption Refrigerator

Symbols

$\dot{m}_a$	Air mass flow rate (kg/s)
P	Electrical power (W)
T_a	Inlet air temperature (°C)
T_w	Inlet water temperature (°C)
η_d	Dehumidifier efficiency (%)

Subscripts

a	Air
fw	Freshwater
d	Dehumidifier
h	Humidifier

water treatment solution [6-8]. Striking the right balance between cost, energy use, and environmental sustainability is crucial for ensuring long-term freshwater security in water-stressed regions.

Technologies for producing freshwater can be divided into two critical categories, membrane technology and thermal technology. MED (Multi-Effect Distillation) [9], MSF (Multi-Stage Flash), and RO (Reverse Osmosis) systems are among the most important and widely used water desalination methods [10]. RO systems belong to the category of membrane technologies, and MED and MSF systems belong to thermal technologies. RO systems have the most significant freshwater production capacity among all freshwater production technologies. Notably, RO technology accounts for 69 % of freshwater production worldwide [11]. However, despite the high production capacity of RO technology, it consumes considerable electrical energy to produce freshwater, causing high-cost freshwater production [12]. In addition, in this method, only solutes and fine particles can be separated from water, while many microbes and toxins dissolved in the water remain, despite the efforts of researchers [13]. Thermal desalination using MSF and MED provides about 18 % and 7 % % of the global freshwater production capacity, respectively [14,15]. Although they have a lower production capacity than the RO method, they are in the category of widely used technologies that are used to produce water at a high capacity and for a large region with a high population [15]. These technologies require energy sources with high temperatures, for this purpose, they are generally installed next to thermal power plants to produce electricity so that waste heat in power plants can be used to run these systems [16,17]. Therefore, the technologies mentioned above cannot be used to produce fresh water for small, decentralized and remote regions.

Nowadays, while the lack of freshwater resources is becoming a concerning issue, the world is also struggling with the shortage of energy resources and environmental challenges. Therefore, proposing a sustainable method to establish a balance between the production of fresh water and energy is vital. Meanwhile, renewable energy can be a suitable solution because it has fewer environmental effects and can address the energy shortage problem. In this regard, many researchers worldwide studied combining renewable energy, such as solar energy [18,19] and geothermal energy, with desalination systems [20,21]. Solar desalination is a process in which solar energy separates salt from seawater. This method is precisely similar to creating rain in nature [22]. There are many technologies in the field of solar desalination, which can be divided into two categories: direct and indirect solar desalination. Among the most important examples of indirect solar desalination, we can mention MED, MSF and RO desalination, in which the required energy is supplied indirectly from the solar. Among the types of direct solar desalination plants, the most important ones are SSD [23] and HDH desalination plants [24]. Chauhan et al. [21] in their review study on solar desalination, made a comparison between SSD and HDH desalination. Their comparison shows that HDH systems have far more freshwater production capacity ($\frac{L}{m^2.day}$) than SSD desalination. In that study, the highest amount of water production by the HDH system was equal to 44 $\frac{L}{m^2.day}$ and the highest amount of water production by the SSD system was equal to 18 $\frac{L}{m^2.day}$. Therefore, the solar HDH system occupies a smaller region and has far lower maintenance costs than SSD.

In recent years, many studies have been conducted on the combination of HDH systems with other systems [25-27]. Alqaed et al. [28] numerically investigated three unique solar-driven poly-generation systems that combine an organic Rankine cycle (ORC), a HDH, and a desiccant cooling system (DCS). These proposed systems provide electricity, space cooling, local heating, and potable water for small to medium-scale buildings. Using n-octane as the working fluid in the ORC, they examined the impact of operational conditions on system productivity and performance. The results showed that the IS-I system achieved the best performance, and maximum values of electrical power, fresh water production rate, space cooling, local heating, and thermal gain output ratio (TGOR) were obtained for the different systems. This study demonstrates that solar-driven poly-generation systems can be a promising solution for the simultaneous provision of energy, cooling, heating, and water in buildings.

One of the important features of the HDH system is its suitability for remote regions with small and decentralized populations, the ability to operate with low-temperature energy sources, especially solar energy [29], low maintenance costs, and its reliability [1,3,24]. HDH water desalination systems can be started by solar energy or other heat sources, such as waste heat from power cycles, refrigeration and geothermal energy [30]. These systems comprise three vital components: a humidifier (HUM), a dehumidifier (DHU), and a heater [31]. The operational process of the HDH system involves heating either saline water or air, which are then separately introduced into the HUM. There, the saline water and air are in direct contact with each other, resulting in humid absorption by the air and humid air is produced. The humid air is condensed in the DHU, producing fresh water. [1,3]. There are different configurations for HDH systems [30]. Depending on the air or water flow is open or closed, different configurations can be introduced. Therefore, there are four different configurations, closed water-closed air (CWCA), closed water-open air (CWOA), open water-open air (OWOA) and open water-closed air (OWCA). In closed-water systems, the concentration of salt in the water gradually rises when more seawater is introduced, leading to a decrease in system performance and an increase in maintenance expenses [32]. Also, three different configurations were considered for HDH system heating: air heating, water heating or simultaneous heating of air and water. Lawal et al. [30] in their review studies, showed, the utilization of air heating in the HDH cycle results in the lowest water production cost and the highest GOR

value, While the use of water heating has a high freshwater production rate and acceptable cost and GOR. They also showed that the simultaneous use of air and water heating has a high cost and low production and GOR. Aghajani et al. [1] in their study, proposed an HDH system with air heating for humid regions to increase its humidification by increasing the T_a. They suggested the closed water-open air system. In their research, Habib [31] conducted a thermodynamic analysis of a desalination system using the humidification–dehumidification (HDH) process with semi-open-air (SOA) circulation. The system, which derives energy from solar sources, is applicable in both arid and humid conditions. The efficiency remains consistent regardless of air circulation mode, but water heating improves overall system efficiency. The highest GOR is achieved at specific MFR ratios, and the system performs best in semi-open-air mode at 50 °C.

Most solar HDH systems use condensers to dehumidify the air in the DHU, where the fluid passing through the condenser tubes is seawater before heating and spraying in the HUM [33-36]. In recent years, researchers have proposed and investigated different models of DHUs. Using the cooling of refrigeration cycles to dehumidify the air is an attractive idea that most researchers have investigated. Kuterbekov et al. [37] evaluated a HDH desalination system coupled with thermoelectric cooling. They investigated the impact of varying seawater mass flow rate (SWMFR) and air mass flow rate (AMFR) on the performance characteristics of the system, such as gained output ratio (GOR), coefficient of performance (COP), freshwater generation, and dehumidifier efficiency. The results showed that the performance of the system was significantly influenced by the SWMFR and AMFR, and the ideal values for these parameters were identified. Additionally, the experimental evaluation demonstrated the capability of the integrated HDH desalination with thermoelectric cooling system as a highly efficient and economically viable approach for desalination, particularly in regions with limited water resources. Rezaei et al. [3] proposed a model using thermoelectric modules for dehumidification. Saeed Dehghan et al. [38] introduced a hybrid model of high-temp. electrolysis (HDH) combined with a vapor compression refrigeration (VCR) cycle. The freshwater that was generated underwent cooling through a VCR evaporator and was subsequently reintroduced into the DHU through spraying. When humid air comes into touch with cold freshwater particles, the moisture in the air is condensed and more freshwater is created. The waste heat from the VCR condenser was utilized to heat the water before spraying it into the HUM. Moreover, Lawal et al. [39,40] proposed a model of HDH with a VCR. Their proposed model used refrigeration cooling to cool the sea water before entering the DHU condenser tubes. The cooled sea water enters the condenser tubes, and after dehumidifying the air, it enters the heater. In the heater, waste heat from the condenser of the VCR is used. After heating the sea water, this water is sprayed in the HUM unit and causes the air to be humidified. They also studied air heating instead of water heating and compared the results. Further, M. Shojaei et al. [41] presented a model similar to Lawal et al. [40] with the difference that waste heat from the condenser of the VCR was used only for air heating. Also, a direct solar heater was used in the HUM to increase the evaporation rate. In this case, they achieved a maximum GOR of 2, while Lawal et al. [40] achieved a GOR of more than 10.

HDH desalination systems can be particularly advantageous in humid regions due to the high moisture content in the air. In these areas, the air is often already near the point of saturation at typical ambient temperatures. By raising the temperature of the air, a greater amount of humidity can be introduced and absorbed by the air stream. Therefore, when implementing HDH systems in humid climates, it can be beneficial to prioritize the use of an air heater over other heating methods [31]. Utilizing seawater in the condenser tubes of the DHU can diminish the system's effectiveness and reduce freshwater generation. This is because the elevated dew point temperature of the moist air reduces the temperature differential between the DHU and the air stream. To address this issue and enhance the dehumidification process, it is necessary to increase the temperature difference between the DHU and the humid air. One approach to achieve this is through the integration of refrigeration cycles with the HDH system. Combining HDH desalination with a VCR system has been explored by researchers [42]. However, VCR-based hybrid systems typically require additional electrical energy to operate, which may not be readily available in remote or off-grid locations. In contrast, integrating the HDH system with a vapor absorption refrigeration (VAR) cycle is a more appealing option. Unlike the VCR cycle, the VAR cycle operates solely on thermal energy, without the need for electrical input. This allows the VAR-HDH hybrid system to be powered by solar heat, which can be utilized as the primary energy source to initiate the cycle. The key advantage of the VAR-HDH integration is that it enables the system to harness the cooling capacity of the VAR cycle to enhance the dehumidification process in the HDH unit. The VAR evaporator can be directly employed as the condenser in the DHU, effectively increasing the temperature difference between the humid air and the dehumidification surface. This, in turn, improves the system's freshwater production efficiency and overall performance. Furthermore, the use of solar energy as the primary power source for the VAR-HDH hybrid system aligns well with the goals of developing sustainable and renewable-powered desalination technologies, particularly in remote or off-grid locations where access to reliable electricity may be limited.

In this study, an innovative hybrid HDH desalination system specifically designed for humid regions was proposed. The system directly integrates a VAR unit and PV panels to enhance performance. A prototype was constructed and experimentally evaluated. The primary objective was to determine the optimal air mass flow rate ($\dot{m}_a$), corresponding to the air temperature exiting the solar heater. By adjusting $\dot{m}_a$ optimally, the system achieves maximum T_a entering the HUM throughout the day. This consideration is crucial, as humid regions often have near-saturation air. Increasing the air temperature entering the HUM allows for greater humidity absorption. The hybrid system operates on solar energy during daylight hours, producing freshwater, and switches to grid electricity during unfavorable conditions. PV panels supply energy for components like the pump, blower, and VAR generator. Excess PV energy is stored in a battery. In the combined cycle, air heated by the solar-electric air heater and seawater is sprayed into the humidifying chamber, producing humid air. This air enters the DHU, where it contacts the VAR evaporator surface, resulting in freshwater production. The integrated HDH-VAR-PV system is novel and will be thoroughly evaluated. Testing occurred in Mangystau City, a coastal and humid region in Kazakhstan. Key input parameters, including air inlet temperature and ṁa, impact system performance metrics such as freshwater production rate, GOR, COP, dehumidifier efficiency, and recovery ratio (RR). Additionally, an economic analysis was conducted.

2. Methodology

2.1. Experimental setup

This study introduces a novel hybrid desalination plant model, which was prototyped and evaluated for performance parameters in the solar energy laboratory at Mangystau, Kazakhstan (Fig. 1). The HDH desalination system operates as an OWOA system and uses air heating to warm the air entering the HUM. The air heating in this model is hybrid, utilizing a solar heater during the day when solar radiation is sufficient and an electric heater at night or on days with insufficient solar radiation. Ambient air is brought into the heater by the blower. and then flows through an insulated channel into the HUM. Sea water is sprayed into the HUM chamber from the top by a pump. The heated air passes over the fine particles of seawater, causing it to evaporate and produce humid air. The excess sea water is removed from the HUM and returned to its source. The humid air produced in this step is then directed through an insulation channel into the DHU, where the VAR evaporator surface is used as the condenser surface. The humid air is condensed on the cold surface of the VAR evaporator, producing fresh water, which is then discharged from the DHU. An electric heater is used for the VAR

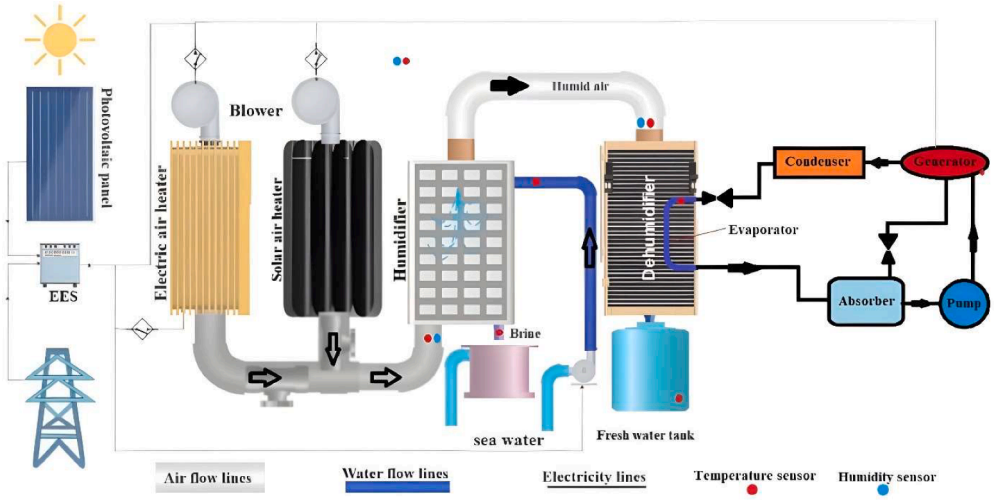

Fig. 1. Schematic diagram of experimental apparatus.

generator in this study. the proposed model consists of equipment such as a pump, blower, electric air heater, and VAR generator heater that require electricity to operate. A photovoltaic panel is installed along with an electric energy storage system so that it can supply the electricity required by the system during the day and, in addition, store the excess electricity produced in the system. It is also possible to use the city's electricity to supply the required electricity in case of a shortage of electric energy produced by solar radiation and energy stored in the battery. Therefore, this system can produce fresh water 24 h a day. A schematic of the proposed model is presented in Fig. 1. The specifications of all equipment are given in Table 1.

2.2. Research and testing environment

The experimental investigations were conducted in the coastal city of Mangystau, situated adjacent to the Caspian Sea in Kazakhstan. Mangystau serves as a compelling test environment due to its distinct climatic features, characterized by high humidity levels, particularly during the summer season. The city's proximity to the Caspian Sea contributes significantly to its elevated humidity, making it an ideal location for evaluating the performance of the proposed humidifier-dehumidifier (HDH) desalination system under moist conditions. Mangystau is geographically positioned near the Caspian Sea's shoreline, experiencing a coastal climate that influences its weather patterns. The city encounters a humid climate, with notable moisture content in the air, especially in the summer months. The Caspian Sea's influence on Mangystau's climate enhances the atmospheric humidity, creating conditions conducive to assessing desalination technologies designed for moisture-rich environments. During the summer season, Mangystau experiences exceptionally high humidity levels, reaching peaks that pose challenges for traditional desalination methods. The humid conditions offer a rigorous testing ground for the HDH system, allowing researchers to gauge its effectiveness in extracting freshwater from air with elevated moisture content. The experimental setup in Mangystau aims to simulate real-world conditions where humidity plays a crucial role in freshwater production. The HDH system's performance metrics, including COP, GOR, RR, and DHU Efficiency, are scrutinized under these specific climatic influences. Table 2 shows the monthly average temperature (in degrees Celsius) and relative humidity (in percentage) for the city of Mangystau:

Table 1
Specifications of system components.

Specifications	Components
Maximum power: 150 W	Electric air heater
Dimensions 100 × 200 mm, angle 40 ° to the horizon	Solar air heater
Dimensions of 1500 × 500 × 600 mm, steel body, insulated by glass fibers	Humidifier
Refrigerant: ammonia absorbent: water The single-effect, generator with an electric heater	Vapor absorption refrigerator (VAR)
A U-shaped tube 500 mm long and 22 mm in diameter is covered by an aluminum heat sink. (The whole assembly is inside a composite shell insulated with glass fibers.)	Dehumidifier (vapor absorption refrigeration evaporator)
Handmade blower, maximum power 20 W, with a 250 mm impeller diameter, with the ability to adjust the speed to create a mass flow in the range of 0.001 to 0.01 kg/s.	Blower
Household water purifier pump, 12 Vs, output pressure 100 psi, maximum flow rate 2 L/min	Pump
Cylindrical tank with a volume of 5 liters	Fresh water tank
Dimensions 1530 × 760 mm, maximum output power 250 W	Photovoltaic panel
A channel with a circular cross-section of aluminum foil, 100 mm in diameter. Insulated by glass fibers	Air channel

2.3. Experimental test process

This study aims to introduce a novel hybrid HDH desalination system model that is suitable for humid regions and directly integrated with absorption cooling systems and photovoltaic panels. The proposed HDH desalination system utilizes a hybrid solar-electric air heater to warm the inlet air for the humidifier. The air heater is designed to operate on

Table 2
Average temperature and relative humidity for the city of Mangystau.

Month	Temperature (°C)	Relative Humidity (%)
January	−5.6	84
February	−4.9	84
March	0.3	84
April	9.1	75
May	16.4	67
June	**22.1**	**57**
July	**25.3**	**51**
August	**24.4**	**53**
September	18.3	60
October	10.9	72
November	3.8	82
December	−2.4	85
Annual Average	9.8	71

solar energy during favorable daylight hours and switch to grid electricity during periods of insufficient solar radiation or nighttime conditions. This hybrid configuration ensures a continuous supply of heated air to the system, maintaining its operational stability and freshwater production capacity. However, it is essential to consider scenarios where the available solar power may not be sufficient to meet the heating requirements of the inlet air. In such cases, the system's reliance on grid electricity increases, affecting its overall energy consumption and operational costs. The variation in air heating by the heater can be influenced by several factors, including the intensity of solar radiation, the efficiency of the PV panels, and the capacity of the energy storage system.

During periods of low solar radiation or cloud cover, the PV panels may not generate enough electricity to power the air heater adequately. In these situations, the system will draw more electricity from the grid to compensate for the deficit in solar power. The increased reliance on grid electricity can lead to higher operational costs and a reduced environmental benefit of the system. To mitigate the impact of insufficient solar power on the system's performance, several strategies can be employed. One approach is to optimize the size and efficiency of the PV panels to maximize their electricity generation potential. This can be achieved by selecting high-quality PV modules with improved conversion efficiencies and ensuring proper installation and orientation to capture maximum solar radiation.

Another strategy is to incorporate a robust energy storage system, such as high-capacity batteries, to store excess solar energy generated during peak sunlight hours. The stored energy can be utilized to power the air heater during periods of low solar radiation or at night, reducing the system's dependence on grid electricity.

Furthermore, implementing an intelligent control system that can dynamically adjust the air heater's power input based on the available solar energy and the system's heating requirements can help optimize the use of solar and grid electricity. The control system can prioritize the use of solar power when available and seamlessly switch to grid electricity when necessary, ensuring a stable and efficient operation of the HDH desalination system. In conclusion, the variation in air heating by the heater in the proposed HDH desalination system is influenced by the availability of solar power. Scenarios with insufficient solar radiation can lead to increased reliance on grid electricity, affecting the system's energy consumption and operational costs. To address this challenge, strategies such as optimizing PV panel size and efficiency, incorporating robust energy storage, and implementing intelligent control systems can be employed to maximize the utilization of solar energy and minimize the impact of insufficient solar power on the system's performance.

To evaluate and better understand this new system and achieve the optimal $\dot{m}_a$, a sample of this system was made and experimentally evaluated. The main goal of evaluating this system is to determine the optimal $\dot{m}_a$, proportional to the outlet T_a of the solar collector. A prototype was made and located in Mangystau, one of the coastal and humid regions of Kazakhstan. At first, to identify the climatic capacities of the region, a sample of solar air heater was made based on the studies of Akhbari et al. [36]. This solar collector was tested in July, in sunny, semi-cloudy, and cloudy weather conditions. The results show that the maximum outlet T_a from the collector is obtained on sunny days, reaching 56 °C at $\dot{m}_a$ of 0.0039 kg/s. In the worst-case scenario, which was related to a cloudy day, the outlet T_a from the collector reaches 32 °C at $\dot{m}_a$ of 0.007 kg/s.

To determine the optimal $\dot{m}_a$ at different outlet T_a from the solar collector, the constructed model was tested in a controlled laboratory condition. In these conditions, by keeping the outlet T_a from the heater constant and changing the $\dot{m}_a$, the system was evaluated, and the optimal $\dot{m}_a$ was determined. For this purpose, electric heaters were used to control the outlet T_a. Two parameters, the $\dot{m}_a$ and the inlet T_a of the HUM (outlet T_a from the solar collector), were considered as the main variables in the experiment, and other variables related to these two main variables were measured and recorded at various points. In the tests, data such as the power of the pump, the blower power, the water flow rate entering the HUM, the ambient temperature and the thermal power input to the absorption refrigeration generator were considered fixed, and their values are given in Table 3. Also, the characteristics of seawater used in the experiment are reported in Table 3.

The experiments were conducted at temperatures of 35, 40, 45, and 50 °C for the inlet T_a to the HUM, with $\dot{m}_a$ ranging from 0.0039 to 0.0071 kg/s. For example, with the outlet T_a from the heater at 35 °C, the system was tested by changing the $\dot{m}_a$ from 0.0039 to 0.0071 kg/s, and the temperature and relative humidity were measured and recorded at various points.

For each $\dot{m}_a$ and inlet T_a, a period of 45 min was spent to reach steady-state conditions, and then the system was maintained at the same temperature and air flow rate for 60 min. During these 60 min, the temperature and relative humidity were measured and recorded at 15-minute intervals, and the amount of produced fresh water was measured using a graduated cylinder.

This intricate journey through controlled experimentation endeavors to decode the nuanced performance of our system, ultimately guiding us towards optimal parameters for heightened efficiency.

2.4. Error analysis

2.4.1. Measurement equipment and calibration

In this research, to measure the required parameters, three types of sensors have been used, namely, temperature sensor, temperature-humidity sensor, and anemometer sensor. Table 4 shows the specifications of the measuring equipment.

To ensure the accuracy and reliability of the measured data, all sensors used in this research were subjected to a calibration process before installation and use. The DS18B20 temperature sensor was calibrated using a calibrated reference thermometer at three different temperature points (0, 25, and 50 °C). At each temperature point, the sensor's output was compared with the actual temperature value, and calibration coefficients were calculated. For the calibration of the DHT22 temperature-humidity sensor, a chamber with controlled humidity and temperature was used. The sensor was exposed to several different temperature and humidity points, and its output was compared with the reference values. Calibration coefficients were calculated for both temperature and humidity parameters. The Anemometer 485 wind speed sensor was calibrated using a calibrated wind tunnel at various wind speeds. The relationship between the frequency of the sensor's output pulses and wind speed was obtained using the calibration data. After completing the calibration process, the obtained coefficients and relationships were applied in the microcontroller's program to ensure that the data measured by the sensors were reported with the highest possible accuracy. The calibration process for each sensor was repeated at least three times to ensure the repeatability of the results.

2.4.2. Uncertainty analysis

Ensuring the accuracy and reliability of measurement data is crucial for a comprehensive understanding and interpretation of experimental results. In this context, an uncertainty analysis has been conducted on the test outcomes under specific inlet conditions, involving an inlet temperature of 35 °C and $\dot{m}_a$ of 0.004 kg/s.

The methodology employs Eqs. (1) to (3) [37], elucidating key

Table 3
Constant parameters during the test.

Specifications	Unit	Value
Mass flow rate of seawater ($\dot{m}_{sw}$)	*Kg/s*	0.005
Vapor absorption refrigeration electric heater power ($\dot{Q}_g$)	*W*	500
Ambient temperature (T_{amb})	*°C*	0
Blower power (P_b)	*W*	20
Pump power (P_p)	*W*	50

Table 4
Specifications of the measuring equipment.

Measurement Tool	Sensor Model	Measurement Range	Accuracy
Temperature Sensor	DS18B20	−55 °C to +125 °C	±0.5 °C in the range of −10 °C to +85 °C
Temperature-Humidity Sensor	DHT22	Temperature: −40 °C to +80 °C Humidity: 0 % to 100 % RH	Temperature: ±0.5 °C Humidity: ±2 % RH
Anemometer Sensor	Anemometer 485	0 to 32 m/s	±0.1 m/s

metrics as showcased in Table 5:

$$\mathbf{s} = \sqrt{\frac{\sum_{\mathbf{i}=1}^{\mathbf{n}} (\mathbf{x_i} - \overline{\mathbf{x}})^2}{(\mathbf{n}-1)}} \tag{1}$$

Where n denotes the number of test repetitions, x_i represents the measured value, $\overline{x}$ is the average of the measured data, and s signifies the standard deviation of the data.

$$u = \frac{s}{\sqrt{n}} \tag{2}$$

$$U = ku_c \times 100 \tag{3}$$

Here, u denotes the uncertainty of the measurement, while U, with the coverage factor $k = 2$, signifies the combined uncertainty.

The reliability of the experimental data surpasses the 94 % threshold, affirming the robustness and trustworthiness of the measurement equipment utilized in our proposed system. This meticulous uncertainty analysis enhances the credibility of the study's findings and fosters a more nuanced interpretation of the experimental results.

2.5. Performance parameters

The performance of the proposed desalination model was evaluated by calculating parameters such as COP, produced freshwater flow rate, η_d, RR and GOR based on the measured values.

$$COP = \frac{\dot{Q}_e}{\dot{Q}_{collector} + P_p + P_b + \dot{Q}_g} \tag{4}$$

In the above equation, $\dot{Q}_e$ is the cooling produced in the DHU, $\dot{Q}_g$ is the electric power of the VAR generator, P_p is the electric power of the pump, P_b is the electric power of the blower and $\dot{Q}_{collector}$ is the thermal power transferred to the air by the solar air heater. $\dot{Q}_e$ and $\dot{Q}_{collector}$ is obtained from the following equations.

$$\dot{Q}_e = \left(\dot{m}_{fwp} \times h_{fg}\right) + \dot{m}_a\left(h_{o,d} - h_{i,d}\right) \tag{5}$$

$$\dot{Q}_{collector} = \dot{m}_a C_p \left(T_{i,h} - T_{amb}\right) \tag{6}$$

T_{amb} is the ambient temperature, C_p is the specific heat capacity of air and $\dot{m}_{fwp}$ is the mass flow rate of water production.

GOR, the ratio of the latent heat of evaporation of fresh water produced to the total energy input to the system from the heat source, is defined and calculated from Eq. (7).

$$\mathrm{GOR} = \frac{\dot{m}_{fwp} \times h_{fg}}{\dot{Q}_{collector} + \dot{Q}_{PV}} \tag{7}$$

h_{fg} is the latent enthalpy of water evaporation at atmospheric pressure and $\dot{Q}_{PV}$ is the electric power produced by the photovoltaic panel.

RR is defined as the ratio of the produced freshwater flow rate to the incoming seawater flow rate and is calculated using Eq. (8). RR indicates the percentage of incoming seawater that has been converted into fresh water.

$$RR = \frac{\dot{m}_{fwp}}{\dot{m}_{sw}} \times 100 \tag{8}$$

Dehumidification efficiency(η_d) [43,44]:

$$= \frac{\left(\omega_{i,d} - \omega_{o,d}\right)}{\left(\omega_{i,d} - \omega_{o,d,s}\right)} \tag{9}$$

The values of P_b, P_b, $\dot{Q}_g$, T_{amb} and $\dot{m}_{sw}$ were constant during all experiments and are listed in Table 3. Other values were measured during the experiment.

3. Results and discussion

In this study, the effect of two important variables, inlet T_a to the evaporator ($T_{a,i,\ Dh}$) and $\dot{m}_a$, on the performance characteristics of the proposed system, has been experimentally investigated. In this section, the experimental results are analyzed. Since the desired HDH desalination system utilizes the evaporator of the VAR for dehumidification, it is necessary to first examine the performance of the VAR system at different inlet T_a to the evaporator. In the experiment, dry air with temperatures ranging from 20 to 50 °C was introduced into the evaporator. Subsequently, the temperature of the air exiting the evaporator was measured. Fig. 2 shows that as the inlet T_a to the VAR evaporator increases, the coefficient of performance (COP) also increases in a nearly linear manner. The accuracy of this trend can be found in the studies of Dawn Sun et al. [45] (Fig. 3) and also Z. CREPINSEK et al. [46]. Fig. 3, which illustrates the variation of the COP as a function of the evaporator surface temperature in their studies, reveals a nearly linear trend. This observed trend is consistent with the results obtained from the experimental testing of the system in the present study, as depicted in Fig. 2. The close agreement between the two sets of data validates the experimental methodology employed in this work and reinforces the reliability of the findings.

The physical reason for this behavior can be explained as follows: with an increase in the inlet T_a to the evaporator, the temperature difference between the air and the cooling fluid in the evaporator increases. This higher temperature difference enhances the driving force for heat transfer and leads to more evaporation in the evaporator. As a result, the cooling capacity of the evaporator and consequently the COP of the absorption chiller increase. Moreover, considering that the electric heating power of the VAR generator has a constant value, increasing the COP means increasing the cooling production in the evaporator section. This implies that at higher inlet T_a, the VAR evaporator can dehumidify more humid air. Therefore, increasing the inlet T_a not only improves the performance of the absorption chiller but also indirectly enhances the ability of the HDH system to produce fresh water.

However, it should be noted that an excessive increase in the inlet T_a may have negative effects on the system, such as increased scale

Table 5
Uncertainty analysis of measurement equipment in the proposed system.

Variable	1	2	3	4	5	$\overline{x}$	s	u	U
$T_{a,o,\ d}(^{\circ}C)$	25.91	25.93	25.95	25.93	25.96	25.936	0.0195	0.0087	1.7 %
$\dot{m}_{sw}\ (L/min)$	0.54	0.54	0.55	0.53	0.54	0.54	0.007	0.003	0.6 %
$V_a(m/s)$	4.55	4.50	3.63	4.61	4.49	4.556	0.063	0.282	5.6 %

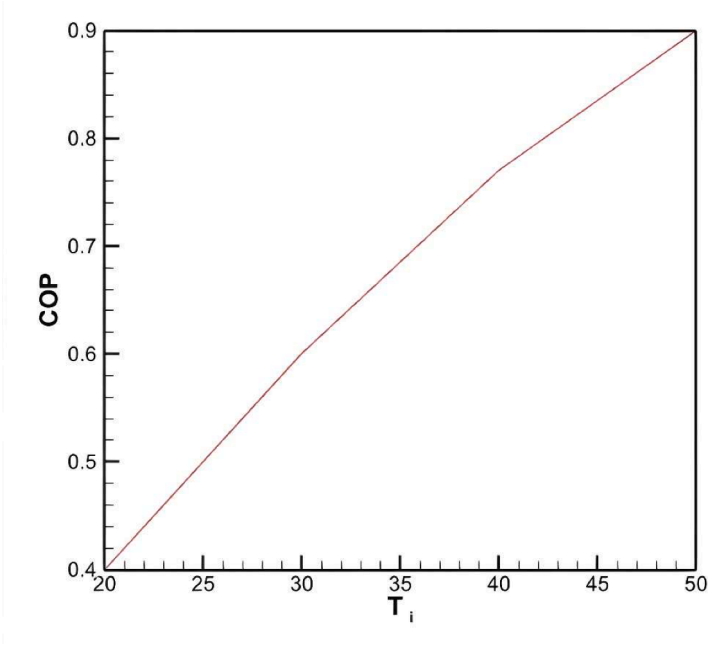

Fig. 2. COP changes according to the temperature of the incoming air in the present study (for water-ammonia absorption refrigeration, single effect).

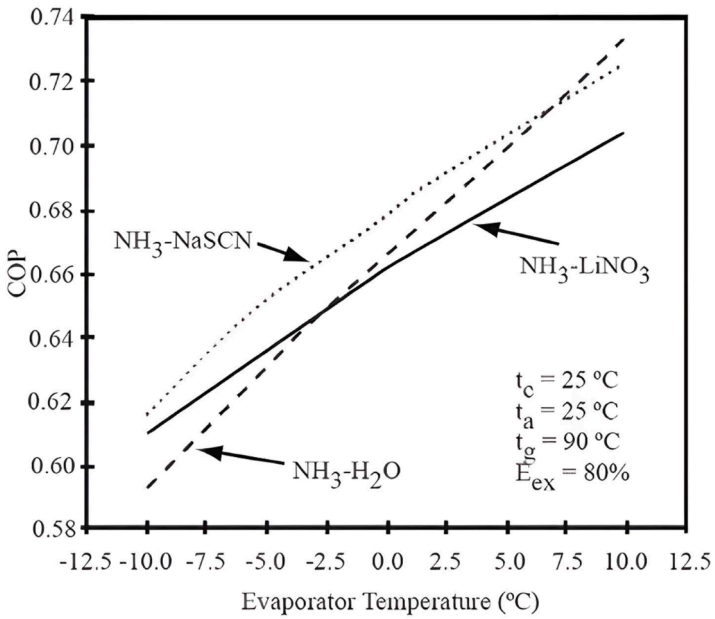

Fig. 3. The trend of changes in COP according to the temperature of the air entering it in the study of Dawn Sun et al. [45].

formation and corrosion in the evaporator. Additionally, very high $T_a$can reduce the relative humidity of the air, which may adversely affect the dehumidification process in the HDH system. Therefore, it is essential to determine the optimal range of inlet T_a to achieve the best overall system performance.

According to the test findings, it was observed that raising the inlet temperature of the HUM at all $\dot{m}_a$ leads to an increase in the inlet T_a of the DHU (Fig. 4). This behavior can be attributed to the enhanced heat and mass transfer processes within the humidifier at higher inlet T_a. As the inlet T_a increases, the water vapor carrying capacity of the air also increases, allowing more moisture to be absorbed by the air stream in the humidifier. Consequently, the humid air leaving the humidifier and entering the dehumidifier has a higher temperature and moisture content. Based on the COP data obtained from the test conducted with dry air (Fig. 2), it is expected that the COP of the main desalination system will increase when the temperature of the humid air entering the dehumidifier rises. The graph depicted in Fig. 5 accurately illustrates this trend. It is evident that in the proposed desalination system, raising the temperature of the air entering the humidifier leads to a consistent and proportional increase in COP, regardless of the $\dot{m}$. This can be explained by the fact that higher inlet T_a in the humidifier result in higher inlet $T_a$in the dehumidifier, which in turn enhances the performance of the VAR evaporator used for dehumidification. As discussed earlier, higher inlet T_a in the VAR evaporator lead to increased cooling capacity and COP.

Furthermore, it is observed that this linear trend becomes more pronounced with higher $\dot{m}$. This can be attributed to the increased heat and mass transfer rates at higher flow rates. As the $\dot{m}$ increases, more air

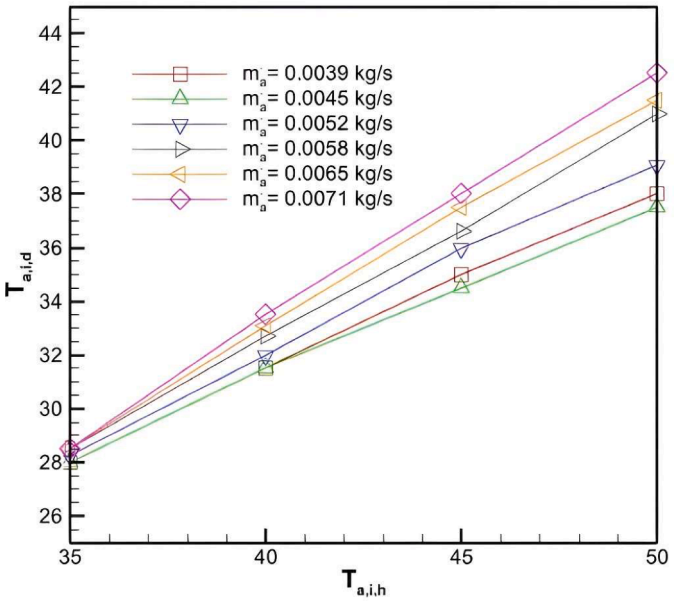

Fig. 4. Variation in $T_{a,i,\ d}$ with $T_{a,i,\ h}(^{\circ}C)$.

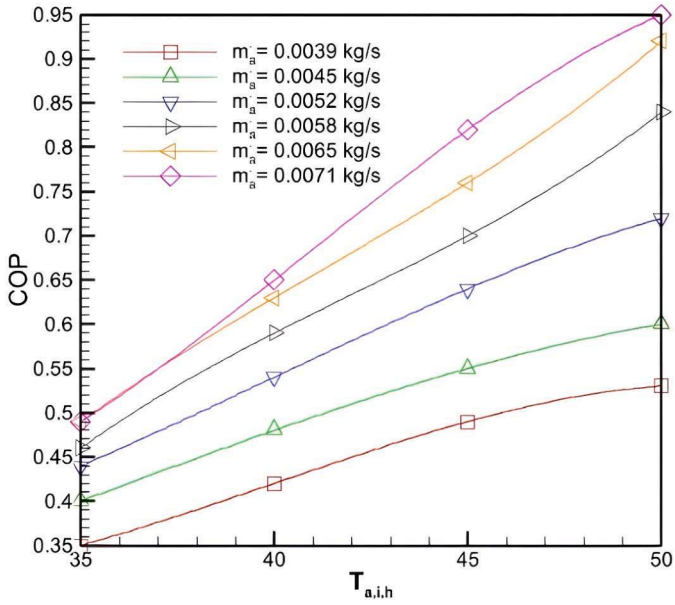

Fig. 5. Variation in *COP* with $T_{a,i,\ h}(^{\circ}C)$.

is available for humidification and dehumidification processes, leading to enhanced system performance. The combination of high inlet $T_a$and high $\dot{m}$ results in the highest COP values. The maximum COP achieved in these experiments is 0.95, obtained at an inlet T_a of 50 °C and a $\dot{m}$ of 0.0071 kg/s. This indicates that the proposed desalination system operates most efficiently under these conditions. However, it is important to note that operating at excessively high temperatures may lead to practical challenges such as increased scaling and corrosion in the system components. Therefore, while higher temperatures favor better performance, it is crucial to find an optimal operating range that balances efficiency with system durability and maintenance requirements.

In summary, the experimental results demonstrate that increasing the inlet T_a of the humidifier leads to higher inlet T_a in the dehumidifier, which in turn improves the COP of the proposed desalination system. This trend is consistent across different $\dot{m}$, with higher flow rates amplifying the positive effect of temperature on system performance. The findings highlight the importance of optimizing the operating conditions, particularly the inlet T_a and $\dot{m}$, to maximize the efficiency of the desalination process.

Since the thermal power input to the VAR generator is constant, the increase in COP means an increase in the cooling production in the DHU unit. This is a crucial point because the cooling capacity of the dehumidifier directly influences the amount of water vapor that can be condensed and collected as fresh water. As the COP rises, more cooling is available to remove latent heat from the humid air, leading to enhanced water production.

The main purpose of the constructed system is to produce fresh water. Therefore, it is very important to examine the amount of water production under different conditions. Fig. 6 demonstrates that the rise in $\dot{m}_a$ leads to an increase in the generation of fresh water, following an almost parabolic pattern across all measured temperatures. This behavior can be justified by the fact that an increase in the $\dot{m}$ introduces more humidity into the dehumidifier per unit of time, and as a result, more humidity can be converted into fresh water. However, it is important to note that the slope of the produced freshwater flow rate with respect to $\dot{m}_a$ is positive but decreasing. This trend can be explained by considering the effect of air velocity on heat transfer. As the flow rate increases, the air velocity through the dehumidifier also increases. Higher air velocities reduce the contact time between the humid air and the cooling surface (VAR evaporator), limiting the heat exchange effectiveness. Consequently, the water production rate increases with air flow rate, but with a diminishing slope.

According to Fig. 6, it can be observed that at a constant flow rate, an increase in temperature leads to higher fresh water production. Furthermore, with increasing temperature, the upward trend of fresh water production exhibits a steeper slope with respect to air flow rate. This phenomenon can be attributed to the rise in COP of the system as the temperature increases. A higher COP indicates more effective heat removal from the humid air, resulting in enhanced water condensation and production. From a thermodynamic perspective, increasing the T_a also raises the dew point temperature. As a result, the temperature difference between the humid air and the dehumidifier surface increases, promoting faster heat transfer rates and facilitating increased fresh water production.

The experimental results reveal that the optimal conditions for achieving the highest fresh water production rate occur when the air entering the humidifier is at a temperature of 50 °C and a flow rate of 0.0071 kg/s, yielding an impressive 870 g of fresh water per hour. These findings underscore the significance of operating the system at elevated temperatures and flow rates to maximize water production. However, it is essential to consider the practical limitations and energy requirements associated with maintaining high temperatures and flow rates. Striking a balance between maximizing water production and ensuring the system's energy efficiency and sustainability is crucial for real-world applications.

In conclusion, the experimental investigation highlights the strong influence of inlet T_a and $\dot{m}$ on the performance of the proposed desalination system. Increasing both parameters leads to higher COP values and enhanced fresh water production rates. The results provide valuable insights into optimizing the operating conditions to achieve the best possible performance while considering practical constraints. Further research could focus on exploring alternative system configurations, improving component designs, and investigating the long-term reliability and scalability of the proposed desalination technique.

In summary, the physical and scientific reasons behind the observed trends in fresh water production involve a complex interplay of thermodynamics, psychrometrics, heat and mass transfer, and system design. Understanding these underlying principles is crucial for optimizing the performance of the proposed desalination system and maximizing its fresh water production potential. the air and the efficiency of the dehumidifier in removing moisture from the air depend on factors such as the heat and mass transfer surface areas, materials of

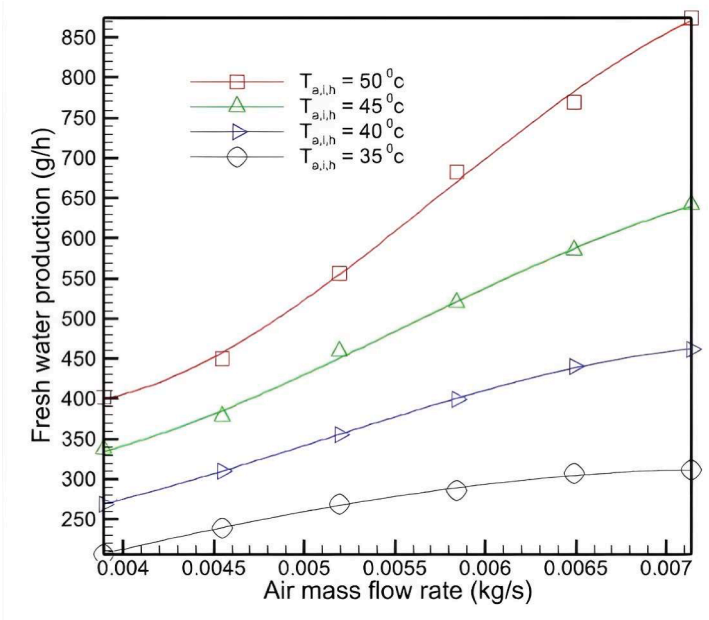

Fig. 6. Variation in Produced fresh water with $\dot{m}_a$.

construction, and flow configurations. Optimizing these design parameters can further enhance the system's performance and fresh water production capacity. In summary, the physical and scientific reasons behind the observed trends in fresh water production involve a complex interplay of thermodynamics, psychrometrics, heat and mass transfer, and system design. Understanding these underlying principles is crucial for optimizing the performance of the proposed desalination system and maximizing its fresh water production potential.

One of the most important performance parameters of the proposed system is the DHU efficiency. According to Fig. 7, with the increase in $\dot{m}_a$, the efficiency of the DHU decreases at all tested temperatures. This decreasing trend exhibits a proportional behavior and occurs more intensely at high temperatures. The observed phenomenon can be explained by considering the interplay between heat transfer and air flow dynamics within the dehumidifier. As the $\dot{m}$ increases, the velocity of the air flow through the dehumidifier also increases. Higher air velocities reduce the residence time of the humid air in contact with the cooling surface (VAR evaporator), thereby diminishing the opportunity for effective heat exchange. Consequently, the humid air spends less time in the dehumidifier, and a smaller portion of its moisture content is condensed and removed. This results in a higher absolute humidity at the DHU outlet compared to lower flow rates.

Moreover, the reduction in heat transfer effectiveness at higher air velocities has a direct impact on the surface temperature of the evaporator. With less effective heat exchange, the evaporator surface becomes colder. The saturated absolute humidity at a temperature equal to the surface temperature of the evaporator, denoted as $\omega_{o,d,\ s}$, decreases as a result of the lower surface temperature. This decrease in $\omega_{o,d,\ s}$ has a

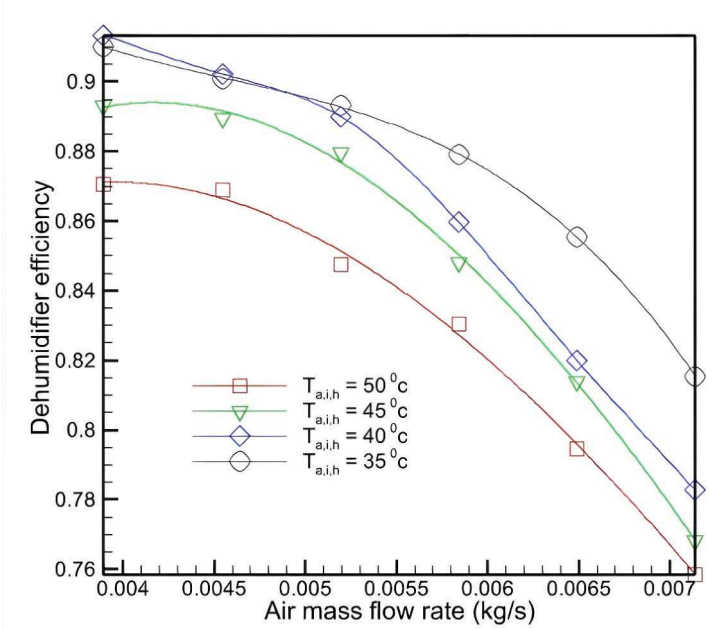

Fig. 7. Variation in DHU efficiency with $\dot{m}_a$.

significant effect on the DHU efficiency, as evident from Eq. (9). Eq. (9) defines the DHU efficiency as the ratio of the actual change in absolute humidity to the maximum possible change in absolute humidity. The denominator of this equation represents the maximum possible change in absolute humidity, calculated as the difference between the inlet absolute humidity $\omega_{i,d}$ and the saturated absolute humidity at the evaporator surface temperature $\omega_{o,d,\ s}$. As $\omega_{o,d,\ s}$ decreases due to the colder evaporator surface, the denominator of Eq. (9) increases. Consequently, for a given actual change in absolute humidity (numerator), the overall DHU efficiency decreases with increasing $\dot{m}$.

The highest DHU efficiency is obtained at a flow rate of 0.0039 kg/s and temperatures of 35 and 40 °C. This observation suggests that there exists an optimal balance between the $\dot{m}$ and the heat transfer effectiveness within the dehumidifier. At lower flow rates, the air has sufficient residence time to undergo effective heat and mass exchange with the cooling surface, resulting in higher dehumidification efficiencies. However, it is important to note that excessively low flow rates may limit the overall fresh water production capacity of the system, as less humid air is processed per unit time. From a thermodynamic perspective, the relationship between the T_a and the DHU efficiency can be understood by considering the driving force for heat and mass transfer. At higher temperatures, the difference between the inlet T_a and the evaporator surface temperature is greater, providing a larger driving force for heat transfer. This enhanced heat transfer potential at higher temperatures contributes to the more intense decrease in DHU efficiency with increasing $\dot{m}$.

In summary, the decrease in DHU efficiency with increasing $\dot{m}_a$ can be attributed to the reduced residence time of the humid air in the dehumidifier and the diminished heat transfer effectiveness at higher air velocities. The colder evaporator surface resulting from the reduced heat transfer leads to a decrease in the saturated absolute humidity at the evaporator surface temperature, which in turn increases the denominator of the efficiency equation and lowers the overall DHU efficiency. The interplay between air flow dynamics, heat transfer, and thermodynamic driving forces governs the observed trends in DHU efficiency, with an optimal balance achieved at lower flow rates and moderate temperatures.

The recovery ratio is an important parameter that quantifies the effectiveness of the desalination system in converting seawater into fresh water. It is defined as the ratio of the amount of fresh water produced to the total amount of seawater entering the system. A higher recovery ratio indicates a more efficient utilization of the input seawater and a greater production of fresh water per unit of seawater processed.

According to the diagram in Fig. 8, the recovery ratio exhibits an upward trend with increasing $\dot{m}_a$ at all tested temperatures. This behavior is similar to the trend observed for the coefficient of performance (COP). The positive correlation between the recovery ratio and $\dot{m}_a$ can be explained by considering the influence of air flow rate on fresh water production and the amount of seawater processed. As discussed earlier, increasing the $\dot{m}_a$ introduces more humid air into the system, leading to higher fresh water production rates. This is because a larger volume of air is available for humidification in the humidifier and subsequent dehumidification in the dehumidifier. Consequently, more water vapor is extracted from the humid air, resulting in increased fresh water production. The numerator of the recovery ratio, which represents the amount of fresh water produced, increases with higher $\dot{m}_a$.

On the other hand, the total amount of seawater entering the system, which forms the denominator of the recovery ratio, remains relatively constant or increases at a slower rate compared to the fresh water production. The seawater intake is primarily determined by the capacity and design of the system, and it may not be directly proportional to the $\dot{m}_a$. As a result, the recovery ratio, which is the ratio of fresh water produced to the total seawater input, increases with increasing $\dot{m}_a$. The similarity between the recovery ratio trend and the COP trend can be attributed to the relationship between fresh water production and the system's energy efficiency. A higher COP indicates that the system is producing more cooling effect (dehumidification) per unit of heat input. This increased cooling effect leads to enhanced fresh water production, as more moisture is extracted from the humid air. Consequently, the recovery ratio, which is directly related to fresh water production, follows a similar trend to the COP.

According to the results presented, the maximum recovery ratio achieved by the desalination system is 4.9 %. This means that up to 4.9 % of the seawater entering the desalination plant can be converted into fresh water under the tested operating conditions. While this recovery ratio may seem relatively low compared to some other desalination technologies, it is important to consider the specific design and operating parameters of the proposed system.

The GOR is another crucial performance parameter examined in this study. GOR represents the ratio of the latent heat of evaporation of the

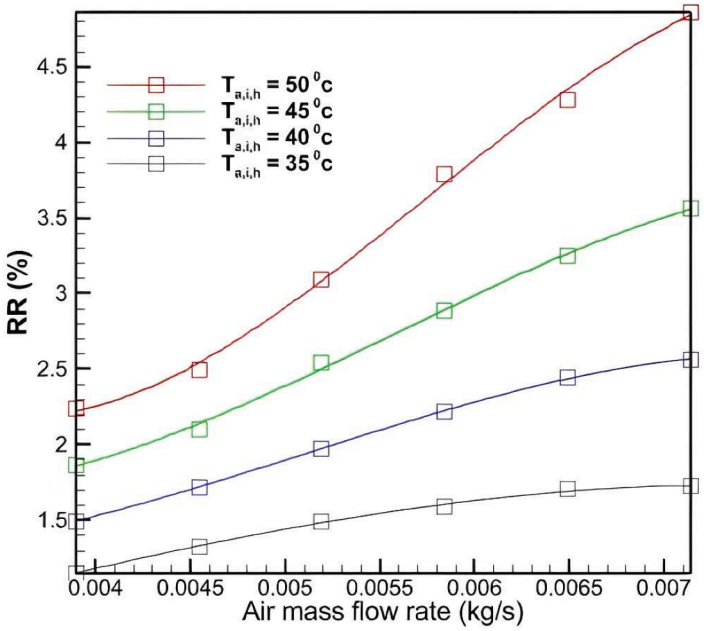

Fig. 8. Variation in Recovery ratio with $\dot{m}_a$.

produced fresh water to the total heat input to the system. It is a measure of the system's efficiency in converting thermal energy into fresh water production. According to the diagram in Fig. 9, GOR exhibits a proportional relationship with the $\dot{m}_a$. As $\dot{m}_a$ increases, the GOR value initially rises, reaches a maximum, and then decreases with further increases in $\dot{m}_a$. This behavior can be explained by considering the interplay between fresh water production and energy consumption. At lower $\dot{m}_a$, the system produces relatively less fresh water due to the limited amount of humid air processed. However, as the flow rate increases, more humid air is introduced into the system, leading to higher fresh water production rates. This increase in fresh water production contributes to the initial rise in GOR. As more latent heat is extracted from the humid air through the dehumidification process, the numerator of the GOR equation (latent heat of evaporation of the produced fresh water) increases, resulting in higher GOR values.

However, beyond a certain optimal flow rate, the GOR reaches a maximum and starts to decrease with further increases in $\dot{m}_a$. This decline in GOR can be attributed to the diminishing returns in fresh water production at higher flow rates. As discussed earlier, increasing the $\dot{m}_a$ reduces the residence time of the humid air in the dehumidifier, limiting the heat and mass transfer effectiveness. Consequently, the incremental gain in fresh water production becomes smaller compared to the increase in energy consumption associated with handling the higher air flow rates. The denominator of the GOR equation (total heat input to the system) continues to rise with increasing $\dot{m}_a$, while the numerator (latent heat of evaporation of the produced fresh water) experiences a slower growth rate. This imbalance leads to the observed decrease in GOR beyond the optimal flow rate.

The influence of temperature on the GOR trend is also noteworthy. At a lower temperature of 35 °C, the increasing and decreasing trend of GOR with respect to $\dot{m}_a$ occurs with a gentler slope, and the maximum GOR is reached at a flow rate of 0.0058 kg/s, with a value of 0.7. As the temperature increases from 35 to 50 °C, the GOR changes exhibit a steeper slope. The maximum GOR values occur at higher flow rates of 0.006, 0.006, and 0.0065 kg/s for temperatures of 40, 45, and 50 °C, respectively, with corresponding GOR values of 1.05, 1.3, and 1.6. This observation suggests that at higher temperatures, the system requires higher $\dot{m}_a$ to achieve optimal efficiency and maximize the GOR. The shift in the optimal flow rate for maximum GOR towards higher values with increasing temperature can be explained by the enhanced heat and mass transfer processes at elevated temperatures. Higher temperatures promote better evaporation in the humidifier and more effective condensation in the dehumidifier. As a result, the system can handle higher $\dot{m}_a$ while still maintaining efficient fresh water production. This is evident from Fig. 6, which shows that the amount of water production increases with increasing flow rate at high temperatures.

In summary, the GOR is a valuable performance parameter that reflects the efficiency of the desalination system in converting thermal energy into fresh water production. The proportional relationship between GOR and $\dot{m}_a$, with the presence of a maximum point, highlights the importance of optimizing the flow rate to achieve the best system efficiency. The influence of temperature on the GOR trend and the optimal flow rate for maximum GOR emphasizes the need to adjust the operating conditions based on the prevailing temperature to ensure optimal performance. By considering the interplay between fresh water production, energy consumption, and the effects of temperature, the proposed desalination system can be operated at its peak efficiency, maximizing the GOR and fresh water output.

The proposed VAR-HDH hybrid desalination system offers several advantages over previous models studied by other researchers. Unlike VCR-based hybrid systems, which require additional electrical energy to operate the refrigeration cycle, the use of a VAR cycle in the present study allows the system to be powered solely by thermal energy, such as that provided by solar heat. This is a particularly attractive feature for remote or off-grid applications where access to reliable electricity may be limited. Furthermore, the integration of the VAR evaporator as the condenser in the HDH dehumidification unit enables a greater temperature difference between the humid air and the cooling surface. This enhanced temperature differential improves the dehumidification efficiency and freshwater production capacity of the system, overcoming the limitations faced by HDH systems that employ seawater in the condenser tubes, especially in humid climates. By harnessing the cooling potential of the VAR cycle to boost the HDH dehumidification process, the proposed hybrid system can achieve higher freshwater yields compared to standalone HDH or VCR-HDH configurations, making it a more viable and sustainable option for water desalination in regions with high ambient humidity.

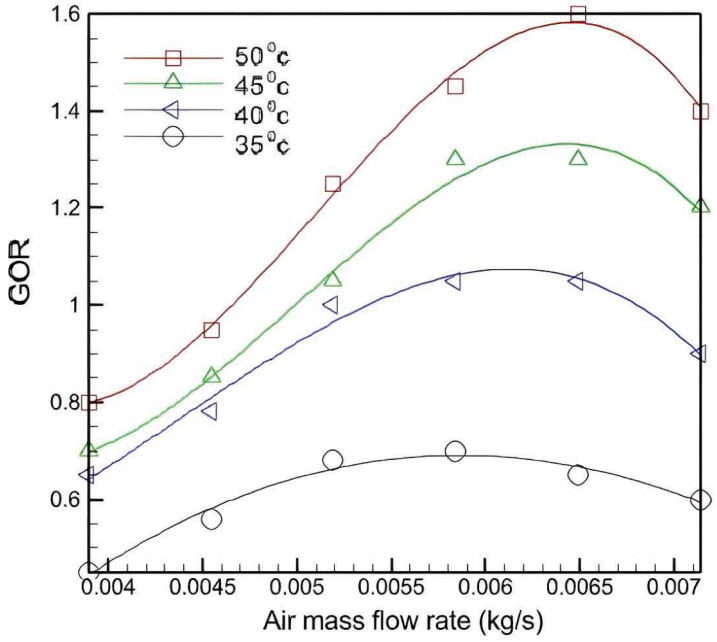

Fig. 9. Variation in GOR with $\dot{m}_a$.

4. Economic analysis

In this study, along with evaluating performance indicators of the system such as fresh water production and GOR, an economic analysis has been conducted as a crucial parameter to assess the efficiency and economic viability of the system. The economic analysis of the proposed system in this study was carried out using the method proposed by Aghajani et al. [1]. Here, more detailed results of the economic analysis, along with explanations, are presented.

For economic analysis, it is assumed that the system operates for 24 h per day, and the annual production period is 365 days. Similarly, the number of years of operation (n) and the interest rate (i) are assumed to be 10 years and 10 %, respectively. The cost of electricity is considered to be CR = 0.039 dollars per kilowatt-hour, based on the rate announced by the Ministry of Energy of Kazakhstan (Table 6).

The cost per kilogram of water has been computed for two methods: complete reliance on solar power and complete reliance on electricity. When the system is running solely on solar power, it operates for 9 h each day and the cost of the solar energy is 0.075 $/kg. During the all-electric operation mode, the duration of work is set at 15 h per day, and the value of CFW_{ele} is 0.094 $/kg. In Kazakhstan, the expense of generating water using electric energy is higher than that of using solar energy, primarily due to the elevated cost of electricity.

4.1. Payback period analysis

The payback period is an important economic indicator that determines the length of time required to recover the initial investment in a project. In this study, the payback period for the proposed HDH desalination system integrated with VAR and PV panels is calculated to assess its economic viability. The payback period can be calculated using the following equation:

$$Payback\ Period\ =\ Initial\ Investment\ /\ Annual\ Net\ Cash\ Flow \tag{10}$$

Where:

Initial Investment is the total capital cost of the system, Annual Net Cash Flow is the difference between the annual revenues and operating costs. To calculate the annual net cash flow, we need to consider the revenue generated from the sale of freshwater and the annual operating costs, which include electricity costs (in the case of electric mode operation) and maintenance costs. Assuming a selling price of freshwater (SPW) of 0.5 $/kg, the annual revenue (AR) can be calculated as follows:

$$AR_{solar}\ =\ AY_{solar}\ \times\ SPW\ =\ 2792\ kg\ \times\ 0.5\frac{\$}{kg} =\ 1396\ \$ per\ year \tag{11}$$

$$AR_{ele} = AY_{ele} \times SPW\ =\ 4654\ kg\ \times\ 0.5\ \$/kg\ =\ 2327\ \$ per\ year \tag{12}$$

The annual net cash flow (ANCF) for both solar and electric modes can be determined by subtracting the respective annual costs from the annual revenue:

$$ANCF_{solar}\ =\ AR_{solar}\ -\ AC_{solar}\ =\ 1396\ \$\ -\ 210.67\ \$\ =\ 1185.33\ \$\ per\ year \tag{13}$$

$$ANCF_{ele}\ =\ AR_{ele}\ -\ AC_{ele}\ =\ 2327\ \$ -\ 439.14\ \$ =\ 1887.86\ \$\ per\ year \tag{14}$$

Now, the payback period for both modes can be calculated:

$$Payback\ Period\_solar\ =\ Initial\ Investment\ /\ ANCF_{\ solar} \\ =\ 1,260/1,185.33\ =\ 1.06\ years \tag{15}$$

$$Payback\ Period\_ele\ =\ Initial\ Investment\ /\ ANCF_{\ ele} =\ 1260/1887.86 \\ =\ 0.67\ years \tag{16}$$

The payback period analysis reveals that the proposed system has a relatively short payback period of approximately 1.06 years when operating in solar mode and 0.67 years in electric mode. This indicates that the initial investment in the system can be recovered within a reasonable timeframe, making it an economically attractive option for freshwater production. It is important to note that the payback period is sensitive to various factors, such as the selling price of freshwater, the cost of electricity, and the efficiency of the system. A higher selling price of freshwater or a lower cost of electricity can reduce the payback period, while a lower selling price or higher electricity costs can increase it.

Furthermore, the payback period analysis does not consider the long-term benefits and potential savings associated with the use of renewable energy sources, such as reduced greenhouse gas emissions and lower environmental impact. These factors, although not directly quantifiable in monetary terms, can enhance the overall economic and environmental viability of the proposed system.

Table 6
Various parameters for economic analysis.

Parameter	Unit	Value
Initial Capital (P)	$	1260
Number of Operating Years (n)	Years	10
Interest Rate (i)	%	10
Operating Hours with Electricity per Day (τ_{ele})	Hours per Day	15
Operating Hours with Solar per Day (τ_{solar})	Hours per Day	9
Electricity Cost (CR)	$/kWh	0.039
Return on Investment Amount (SV = 0.2 × P)	$	252
Capital Recovery Factor ($CRF = \frac{i \times (1+i)^n}{(1+i)^n - 1}$)	–	0.16
Sinking Fund Factor ($SFF = i/[(1+i)^n - 1]$)	–	0.06
First Annual Cost (FAC = P × CRF)	$	201.6
Annual salvage value (ASV = SFF × SV)	$	15.12
Annual maintenance cost (AMC = 0.12 × FAC)	$	24.19
Variable Cost ($ACC\ =\ 365 \times \tau_{ele}\ (P_B\ +\ P_P\ +\ \dot{Q}_g\ +\ \dot{Q}_{\ heater}) \times CR$)	$	228.47
Electricity Annual Cost (AC_{ele} = FAC + AMC + ACC - ASV)	$	439.14
Solar Annual Cost (AC_{solar}= FAC + AMC - ASV)	$	210.67
Daily Production with Electricity (AY_{ele} = $Averagedailyyield \times 365 \times \tau_{ele}$)	kg	4654
Daily Production with Solar ($AY_{solar} = Averagedailyyield \times 365 \times \tau_{solar}$)	kg	2792
Cost per Kilogram of Water Production with Electricity (AC_{ele}/AY_{ele})	$/kg	0.0943
Cost per Kilogram of Water Production with Solar (AC_{solar}/AY_{solar})	$/kg	0.0754

5. Conclusion

This experimental study investigated the performance of a novel HDH desalination system integrated with a VAR and PV panels for humid regions. The system operates in an OWOA configuration, with the VAR evaporator serving as the dehumidifier condenser and PV panels

supplying electrical energy for the VAR's pump, blower, and heater.

Experimental results demonstrated that increasing the $\dot{m}_a$ from 0.0039 kg/s to 0.0071 kg/s led to significant improvements in system performance. Freshwater output increased by 73 %, COP by 35 %, GOR by 100 %, and RR by 75 %. However, dehumidifier efficiency decreased by 20 %. The highest COP of 0.95 was achieved at an inlet T_a of 50 °C and a mass flow rate of 0.0071 kg/s. The maximum freshwater production rate of 870 g/h and a GOR of 1.4 were obtained in the best-case scenario ($\dot{m}_a$= 0.0071 kg/s, inlet T_a = 50 °C), representing a 117 % increase compared to the lowest temperature and flow rate tested. The economic analysis revealed that the cost of CFW for solar and electric operation modes was 0.075 and 0.094 USD/kg, respectively, demonstrating the system's economic viability.

The novelty of this work lies in the integration of HDH desalination with a VAR and PV system, enabling continuous freshwater production even under cloudy or nighttime conditions in humid regions. The VAR evaporator's role as the dehumidifier condenser enhances the system's efficiency and performance.

The findings of this study contribute to the advancement of desalination technologies and provide a promising solution for addressing water scarcity issues in humid regions. The proposed system's ability to produce freshwater under various environmental conditions, coupled with its economic feasibility, makes it an attractive option for sustainable water production.

Future research should focus on further optimizing the system's design and operating parameters to enhance its performance and efficiency. Investigating the long-term durability and scalability of the system would also be valuable for practical implementation. Additionally, exploring the integration of advanced materials and technologies could further improve the system's effectiveness.

In conclusion, the proposed HDH desalination system integrated with a VAR and PV system demonstrates great potential for sustainable freshwater production in humid regions. The experimental results and economic analysis support the system's viability and highlight its novelty in addressing the challenges of water scarcity. With further research and development, this innovative approach could contribute significantly to sustainable water management and alleviate the global water crisis.

CRediT authorship contribution statement

Sherzod Abdullaev: Writing – original draft, Methodology, Investigation, Formal analysis, Conceptualization. **Barno Sayfutdinovna Abdullaeva:** Validation, Software, Resources, Formal analysis, Data curation. **Serikzhan Opakhai:** Writing – review & editing, Visualization, Resources, Methodology, Investigation. **Laith H. Alzubaidi:** Writing – review & editing, Resources, Methodology, Formal analysis, Data curation.

Declaration of competing interest

The authors declare that they have no known competing financial interests or personal relationships that could have appeared to influence the work reported in this paper.

Data availability

Data will be made available on request.

References

[1] S. Aghajani Afghan, et al., An experimental study to apply an absorption refrigeration cycle as a dehumidifier in Humidification-Dehumidification solar desalination system, Iranian (Iranica) J. Energy Environ. (2023).

[2] D.E. McNabb, C.R. Swenson, From water stress to a water crisis. America's Water Crises: The Impact of Drought and Climate Change, Springer, 2023, pp. 29–53.

[3] M. Rezaei Rad, et al., An experimental study to evaluate the performance of an HDH water desalination system with a thermoelectric condenser, Renew. Energy Res. Appl. (2023).

[4] F. Shacheri, et al., Surface dense discharge from rectangular and trapezoidal channels, Flow Meas. Instrum. 1 (87) (2022) 102213.

[5] M. Shammi, M.M. Rahman, M.M. Rahman, Desalination technology for water security, Water Pollut. Remed. (2021) 147–176.

[6] A. Shokri, M. Sanavi Fard, A comprehensive overview of environmental footprints of water desalination and alleviation strategies, Int. J. Environ. Sci. Technol. 20 (2) (2023) 2347–2374.

[7] M.N. Soliman, et al., Environmental impact assessment of desalination plants in the gulf region. Water-Energy-Nexus in the Ecological Transition: Natural-Based Solutions, Advanced Technologies and Best Practices For Environmental Sustainability, Springer, 2022, pp. 173–177.

[8] Y. Cai, et al., Advances in desalination technology and its environmental and economic assessment, J. Clean. Prod. (2023) 136498.

[9] F. Tahir, A. Mabrouk, M. Koç, Heat transfer coefficient estimation of falling film for horizontal tube multi-effect desalination evaporator using CFD, Int. J. Thermofluids 11 (2021) 100101.

[10] N.P.B. Tan, et al., A review of desalination technologies and its impact in the Philippines, Desalination 534 (2022) 115805.

[11] J. Eke, et al., The global status of desalination: an assessment of current desalination technologies, plants and capacity, Desalination 495 (2020) 114633.

[12] J.L. Pearson, et al., Economics and energy consumption of brackish water reverse osmosis desalination: innovations and impacts of feedwater quality, Membranes 11 (8) (2021) 616.

[13] S.G. Salinas-Rodríguez, J.C. Schippers, Introduction to Desalination, 2021.

[14] J. Morón-López, et al., Recycled desalination membranes as a support material for biofilm development: a new approach for microcystin removal during water treatment, Sci. Total Environ. 647 (2019) 785–793.

[15] K. Elsaid, et al., Environmental impact of desalination technologies: a review, Sci. Total Environ. 748 (2020) 141528.

[16] X. Yang, Z. Liu, J. Xia, Optimization and analysis of combined heat and water production system based on a coal-fired power plant, Energy 262 (2023) 125611.

[17] K. Choudhary, M. Agarwal, R. Kumar, An introduction of water desalination exploiting the waste heat and other different renewable source of energy, in: Technology Innovation in Mechanical Engineering: Select Proceedings of TIME 2021, Springer, 2022, pp. 767–772.

[18] S. Vaithilingam, et al., An extensive review on thermodynamic aspect based solar desalination techniques, J. Therm. Anal. Calorim. 145 (2021) 1103–1119.

[19] M.N. AlMallahi, et al., Analysis of solar-powered adsorption desalination systems: current research trends, developments, and future perspectives, Int. J. Thermofluids (2023) 100457.

[20] G.B. Abdelaziz, et al., Hybrid solar desalination systems review, Energy Sour. Part A (2021) 1–31.

[21] V.K. Chauhan, et al., A comprehensive review of direct solar desalination techniques and its advancements, J. Clean. Prod. 284 (2021) 124719.

[22] H. Thakkar, et al., A detailed review on solar desalination techniques, Int. J. Amb. Energy 41 (9) (2020) 1066–1087.

[23] D. Sathish, S. Jegadheeswaran, Evolution and novel accomplishments of solar pond, desalination and pond coupled to desalination systems: a review, J. Therm. Anal. Calorim. 146 (5) (2021) 1923–1969.

[24] T.O. Abimbola, et al., A concise review of major desalination techniques: features and limitations, in: ICCOEE2020: Proceedings of the 6th International Conference on Civil, Offshore and Environmental Engineering (ICCOEE2020), Springer, 2021.

[25] C. Liu, et al., Performance analysis and multi-objective optimization of a novel poly-generation system integrating SOFC/GT with SCO2/HDH/ERC, Appl. Therm. Eng. 238 (2024) 122075.

[26] E. Soleymani, et al., Thermodynamic analysis and examining the effects of parameters in BSR-HDH system using response surface methodology, Renew. Energy (2024) 120430.

[27] H. Nikkhah, B. Beykal, Process design and technoeconomic analysis for zero liquid discharge desalination via LiBr absorption chiller integrated HDH-MEE-MVR system, Desalination 558 (2023) 116643.

[28] S. Alqaed, et al., Performance evaluation of a solar heat-driven poly-generation system for residential buildings using various arrangements of heat recovery units, Energies 15 (22) (2022) 8750.

[29] A. Tiwari, A. Kumar, A comprehensive review on solar thermal desalination systems based on humidification-dehumidification approach, Clean. Technol. Environ. Policy (2023) 1–23.

[30] D.U. Lawal, N.A. Qasem, Humidification-dehumidification desalination systems driven by thermal-based renewable and low-grade energy sources: a critical review, Renew. Sustain. Energy Rev. 125 (2020) 109817.

[31] H.B. Bacha, Thermodynamic comparison of the operation of the HDH system with water heating or air heating in closed water circulation and semi-open-air circulation, Int. J. Thermofluids 21 (2024) 100535.

[32] X. Huang, et al., Performance analysis of a multi-stage humidification–dehumidification desalination system with different salinity levels, Energy Convers. Manage 215 (2020) 112928.

[33] S.H. Soomro, et al., Humidification-dehumidification desalination system powered by simultaneous air-water solar heater, Sustainability 13 (23) (2021) 13491.

[34] I. Tlili, et al., Performance enhancement of a humidification–dehumidification desalination system: a thermodynamic investigation, J. Therm. Anal. Calorim. 140 (2020) 309–319.

[35] K. Garg, et al., Parametric study of the energy efficiency of the HDH desalination unit integrated with nanofluid-based solar collector, J. Therm. Anal. Calorim. 135 (2019) 1465–1478.
[36] A. Mohamed, M.S. Ahmed, A.G. Shahdy, Theoretical and experimental study of a seawater desalination system based on humidification-dehumidification technique, Renew. Energy 152 (2020) 823–834.
[37] K.A. Kuterbekov, et al., Experimental evaluation of combined humidifier-dehumidifier desalination with thermoelectric module for simultaneous use of heating and cooling, Int. J. Thermofluids (2024) 100560.
[38] S. Dehghani, A. Date, A. Akbarzadeh, Performance analysis of a heat pump driven humidification-dehumidification desalination system, Desalination 445 (2018) 95–104.
[39] D.U. Lawal, M.A. Antar, Investigation of heat pump-driven humidification–dehumidification desalination system with energy recovery option, J. Therm. Anal. Calorim. 145 (6) (2021) 3177–3194.
[40] D. Lawal, et al., Humidification-dehumidification desalination system operated by a heat pump, Energy Convers. Manage 161 (2018) 128–140.
[41] M. Shojaei, H. Mortezapour, K. Jafarinaeimi, Experimental investigation of a heat pump-assisted solar humidification–dehumidification desalination system with a free-flow solar humidifier, Int. J. Environ. Sci. Technol. 17 (2020) 2401–2414.
[42] A. Kabeel, M. Abdelgaied, Z. Omara, Experimentally evaluation of split air conditioner integrated with humidification-dehumidification desalination unit for better thermal comfort, produce freshwater, and energy saving, J. Therm. Anal. Calorim. 147 (6) (2022) 4197–4207.
[43] H. Xu, et al., Experimental investigation on a solar assisted heat pump desalination system with humidification-dehumidification, Desalination 437 (2018) 89–99.
[44] H. Xu, Y. Zhao, Y. Dai, Experimental study on a solar assisted heat pump desalination unit with internal heat recovery based on humidification-dehumidification process, Desalination 452 (2019) 247–257.
[45] D.-W. Sun, Comparison of the performances of NH3-H2O, NH3-LiNO3 and NH3-NaSCN absorption refrigeration systems, Energy Convers. Manage 39 (5–6) (1998) 357–368.
[46] Z. Crepinsek, D. Goricanec, J. Krope, Comparison of the performances of absorption refrigeration cycles, WSEAS Trans. Heat Mass Transf. 4 (3) (2009) 65–76.